Pflügers Archiv - European Journal of Physiology (2018) 470:1087–1102
https://doi.org/10.1007/s00424-018-2142-z

ION CHANNELS, RECEPTORS AND TRANSPORTERS

The degenerin region of the human bile acid-sensitive ion channel (BASIC) is involved in channel inhibition by calcium and activation by bile acids

Alexandr V. Ilyaskin[1] · Sonja A. Kirsch[2] · Rainer A. Böckmann[2] · Heinrich Sticht[3] · Christoph Korbmacher[1] · Silke Haerteis[1] · Alexei Diakov[1]

Received: 6 December 2017 / Revised: 12 February 2018 / Accepted: 13 March 2018 / Published online: 27 March 2018

Abstract

The bile acid-sensitive ion channel (BASIC) is a member of the ENaC/degenerin family of ion channels. It is activated by bile acids and inhibited by extracellular Ca^{2+}. The aim of this study was to explore the molecular mechanisms mediating these effects. The modulation of BASIC function by extracellular Ca^{2+} and tauro-deoxycholic acid (t-DCA) was studied in *Xenopus laevis* oocytes heterologously expressing human BASIC using the two-electrode voltage-clamp and outside-out patch-clamp techniques. Substitution of aspartate D444 to alanine or cysteine in the degenerin region of BASIC, a region known to be critically involved in channel gating, resulted in a substantial reduction of BASIC Ca^{2+} sensitivity. Moreover, mutating D444 or the neighboring alanine (A443) to cysteine significantly reduced the t-DCA-mediated BASIC stimulation. A combined molecular docking/simulation approach demonstrated that t-DCA may temporarily form hydrogen bonds with several amino acid residues including D444 in the outer vestibule of the BASIC pore or in the inter-subunit space. By these interactions, t-DCA may stabilize the open state of the channel. Indeed, single-channel recordings provided evidence that t-DCA activates BASIC by stabilizing the open state of the channel, whereas extracellular Ca^{2+} inhibits BASIC by stabilizing its closed state. In conclusion, our results highlight the potential role of the degenerin region as a critical regulatory site involved in the functional interaction of Ca^{2+} and t-DCA with BASIC.

Keywords Degenerin site · Bile acids · BASIC · Tauro-deoxycholic acid · Ca^{2+} · Molecular dynamics (MD) simulations

Introduction

The bile acid-sensitive ion channel (BASIC) belongs to the epithelial sodium channel (ENaC)/degenerin family of non-voltage gated ion channels [26] and was previously known as intestine Na^+ channel (INaC) in human [40] and brain-liver-intestine Na^+ channel (BLINaC) in mouse and rat [38]. Subsequently, the name BASIC was coined to reflect the finding that bile acids activate these channels [29, 49]. BASIC is expressed in the apical membrane of cholangiocytes [49], where bile acids may play a role in regulating BASIC activity under physiological conditions. Recently, it was shown that not only BASIC but also two other members of the ENaC/degenerin family of ion channels (ENaC and ASIC1a—acid-sensing ion channel 1a) can be modulated by bile acids [21, 22, 51]. Therefore, the phenomenon of bile acid sensitivity does not seem to be an exclusive characteristic of BASIC but may be a common feature of ENaC/degenerin channels.

Electronic supplementary material The online version of this article (https://doi.org/10.1007/s00424-018-2142-z) contains supplementary material, which is available to authorized users.

✉ Silke Haerteis
silke.haerteis@fau.de

[1] Institut für Zelluläre und Molekulare Physiologie, Friedrich-Alexander-Universität Erlangen-Nürnberg (FAU), Waldstr. 6, 91054 Erlangen, Germany

[2] Computational Biology, Department Biologie, Friedrich-Alexander-Universität Erlangen-Nürnberg (FAU), Erlangen, Germany

[3] Abteilung für Bioinformatik, Institut für Biochemie, Friedrich-Alexander-Universität Erlangen-Nürnberg (FAU), Erlangen, Germany

BASIC is closely related to the subfamily of acid-sensing ion channels (ASICs) [38, 40] but is not activated by protons. The recently published crystal structures of chicken ASIC1 [2, 3, 10, 16, 24] suggest that also BASIC forms homotrimeric channels in the plasma membrane. An individual BASIC subunit consists of short N and C termini, a large extracellular domain, and two helical transmembrane domains (TMD1, TMD2). Each subunit participates in forming the channel pore with its TMD2, which contains the degenerin site known to be critical for channel gating of ENaC/degenerin ion channels [26].

The molecular mechanism of BASIC activation by bile acids is not yet fully understood. It has been reported that bile acids may affect BASIC function indirectly via an alteration of its membrane lipid environment [41]. However, no specific channel domains sensitive to these alterations were identified, and it was suggested that the entire structure of the channel was crucial for this sensitivity. Recently, we demonstrated that the degenerin region plays a critical role in mediating effects of bile acids on human ENaC and ASIC1a function [21, 22]. Therefore, we hypothesized that BASIC activation by bile acids may involve the degenerin site as well.

Both, BASIC and ASIC1a are inhibited by micromolar concentrations of extracellular Ca^{2+} [29, 35]. For rat ASIC1, it has been reported that the negatively charged aspartate (Asp 432) adjacent to the degenerin site (Gly 431) is crucial for Ca^{2+}-mediated channel inhibition [35]. In contrast, in BASIC, the site responsible for Ca^{2+}-mediated inhibition remains to be identified. Since the TMD2 of BASIC and ASICs share a high degree of homology, the degenerin region may also be involved in BASIC inhibition by Ca^{2+}. Collectively, these findings suggest that bile acids and Ca^{2+} may share a common binding site in the degenerin region of BASIC.

The aim of this study was to investigate whether the degenerin region is involved in BASIC inhibition by Ca^{2+} and activation by bile acids and how interaction of Ca^{2+} and bile acids with the same region may lead to opposite effects on BASIC activity.

Materials and methods

Materials

Diminazene aceturate (Dimi) and sodium tauro-deoxycholate (t-DCA) were purchased from Sigma-Aldrich (Taufkirchen, Germany).

cDNA clones

The cDNA for human BASIC was cloned into pRSSP vector as described previously [49]. Linearized plasmids were used as templates for cRNA synthesis using SP6 RNA polymerases (mMessage mMachine, Ambion, Austin, TX, USA). Mutants in which critical residues in the degenerin region of human BASIC were individually replaced by cysteine, alanine, or serine were generated by site-directed mutagenesis (QuikChange II site-directed mutagenesis kit; Stratagene, La Jolla, CA). Sequences were confirmed by sequence analysis (GATC Biotech, Konstanz, Germany).

Isolation of oocytes and two-electrode voltage-clamp experiments

Isolation of *Xenopus laevis* oocytes and two-electrode voltage-clamp experiments were essentially performed as described previously [13, 18, 19, 21, 37]. Defolliculated stage V–VI oocytes were obtained from ovarian lobes of adult female *Xenopus laevis* in accordance with the principles of German legislation, with approval by the animal welfare officer for the University of Erlangen-Nürnberg, and under the governance of the state veterinary health inspectorate. Animals were anesthetized in 0.2% MS222 (Sigma, Taufkirchen, Germany), and ovarian lobes were obtained by a small abdominal incision. Oocytes were injected with 4 to 8 ng of wild-type (WT) or mutant BASIC cRNA. Injected oocytes were incubated in ND96 solution (in mM: 96 NaCl, 2 KCl, 1.8 $CaCl_2$, 1 $MgCl_2$, 5 HEPES, pH 7.4 with Tris) supplemented with 100 units/ml sodium penicillin and 100 μg/ml streptomycin sulfate. Oocytes were studied 48 h after cRNA injection. Modified ND96 solution was used as standard bath solution (in mM: 96 NaCl, 4 KCl, 1 $CaCl_2$, 1 $MgCl_2$, 10 HEPES, pH 7.4 adjusted with Tris). To obtain a low Ca^{2+} bath solution, 1 mM EGTA was added instead of 1 mM $CaCl_2$ (in mM: 96 NaCl, 4 KCl, 1 EGTA, 1 $MgCl_2$, 10 HEPES, pH 7.4 adjusted with Tris). NaCl (95 mM) was replaced by NMDG-Cl to obtain a low sodium NMDG-Cl bath solution (in mM: 95 NMDG-Cl, 1 NaCl, 4 KCl, 1 $CaCl_2$, 1 $MgCl_2$, 10 HEPES, 7.4 pH adjusted with Tris).

Single-channel recordings in outside-out patches

Single-channel recordings in outside-out membrane patches of BASIC expressing oocytes were performed 48 h after cRNA injection essentially as described previously [11, 12, 21, 29] using conventional patch-clamp technique. Patch pipettes were pulled from borosilicate glass capillaries and had a tip diameter of about 1–1.5 μm after fire polishing. Pipettes were filled with K-gluconate pipette solution (in mM: 90 K-gluconate, 5 NaCl, 2 Mg-ATP, 2 EGTA, and 10 HEPES, pH 7.2 with Tris). Seals were routinely formed in low sodium NMDG-Cl bath solution. In this bath solution, the pipette resistance averaged about 7 MΩ. After seal formation, the NMDG-Cl solution was switched to a NaCl bath solution in which NMDG-Cl (95 mM) was replaced by NaCl (95 mM). For continuous current recordings, the holding potential was set to − 70 mV. Using a 3 M KCl flowing boundary electrode,

the liquid junction (LJ) potential occurring at the pipette/NaCl bath junction was measured to be 12 mV (bath positive) [29]. Thus, at a holding potential of − 70 mV, the effective transpatch potential was − 82 mV. This value is close to the calculated equilibrium potential of Cl^- ($E_{Cl-} = -77.4$ mV) and K^+ ($E_{K+} = -79.4$ mV) under our experimental conditions. Experiments were performed at room temperature (~ 23 °C). Single-channel current data were initially filtered at 2 kHz and sampled at 6 kHz. The current traces were re-filtered at 400 Hz to resolve the single-channel current amplitude (*i*) and to assess channel activity. The latter was derived from binned amplitude histograms as the product *NPo*, where *N* is the number of channels and *Po* is open probability [11, 12, 28, 29]. The apparent number of active channels (apparent *N*) in a patch was determined by visual inspection of current traces. The current level at which all channels are closed was determined in the presence of 10 μM diminazene. Single-channel data were analyzed using the program "Nest-o-Patch" (http://sourceforge.net/projects/nestopatch) written by Dr. V. Nesterov (Institut für Zelluläre und Molekulare Physiologie, Friedrich-Alexander-Universität Erlangen-Nürnberg, Erlangen, Germany).

Homology model of BASIC

No high-resolution structure of human BASIC (hBASIC) has been reported so far. Therefore, homology models of human BASIC were built on the basis of the related acid-sensing ion channel (ASIC1) crystallized in its open state (PDB #4NTW [3]) and desensitized state (PDB #4NYK [16]) using SWISS-MODEL [1, 5, 17, 27]. The corresponding sequence for human BASIC was obtained from the protein database of the National Center for Biotechnology (NCBI) under the accession number Q9NY37. Only the transmembrane helical domains near the channel pore (residues 63–92 and 434–466) were used in all conducted simulations. The sequence similarity for the TMD amounts to 72%.

Molecular docking approach

The homology model of human BASIC TMD was refined by including the polar hydrogen atoms. The grid box defining the docking boundaries was assigned using AutoDockTools 1.5.6 [32, 39]. The structure of t-DCA was extracted from ZINC version 12 database (ZINC ID ZINC04282168; [23]). The t-DCA structure was prepared for docking by defining the rotatable bonds using AutoDockTools 1.5.6. Putative t-DCA binding sites in the transmembrane region of BASIC were predicted using the molecular docking software AutoDock Vina, which uses a knowledge-based empirically weighted scoring function and a global optimization algorithm [45]. Five runs of the program were performed with 20 binding modes generated per run, giving a total number of 100 docked t-DCA modes. Docking results were visually inspected using AutoDockTools. An overlay of the generated modes revealed six prominent clusters of similar modes (see Online Resource 1, Fig. S1). One representative docking model was selected from each cluster (see Online Resource 1, Fig. S2) for further analysis using molecular dynamics (MD) simulations.

Molecular dynamics simulations

The spontaneous binding of dissolved bile acids to hBASIC-TMD embedded in a 1-palmitoyl-2-oleoyl-sn-glycero-3-phosphocholine (POPC) lipid bilayer was investigated in three independent atomistic MD simulations (200 ns each). Further, the stability of six different pre-docked t-DCA-TMD hBASIC configurations was addressed in three 200-ns simulations with differing starting conditions each (in total 18 simulations). Replica simulations of the various studied systems differed in the attributed initial velocities of the atoms.

System preparation

The TMD of the model hBASIC was embedded into a POPC bilayer by first converting the atomistic protein model into the (polarizable) MARTINI [52] coarse-grained (CG) representation using *martinize* [25], followed by addition of POPC molecules, solvent, and counterions with the aid of the membrane builder *insane* [47]. Subsequently, the system was energy minimized and simulated for 40 ns with position restraints on the protein to allow for a relaxation of the lipid environment. The final coarse-grained structure was then converted back to atomistic representation using *backward* [46]. Afterwards, the backmapped atomistic protein was replaced by the hBASIC homology model in order to avoid any bias in the protein structure that may have arisen during the conversion. The system was energy minimized (steepest descent algorithm, 10,000 steps) with frozen protein backbone positions, further simulated for 100 ps in the *NVT* ensemble and 5 ns in the *NpT* ensemble with position restraints on the protein backbone. Simulations were carried out using a combination of Amber14SB [7] and Lipid14 [14] force fields. The Lipid14 force field for lipids was recently shown to combine a very good description of the structure and dynamics of phospholipid membranes with a high computational efficiency [36]. Unless otherwise mentioned, the simulation parameters were chosen equivalent to those used in the production simulations (see below). To summarize, the reference atomistic starting systems consisted of the TMD homology model of BASIC embedded in a POPC membrane (155/160 lipids in the upper/lower layer), counterions, and approximately 22,000 water molecules. To the best of our knowledge, no Amber14 parameters exist for t-DCA. For this reason, we parameterized t-DCA using the parameter set for cholesterol in Lipid14 [14, 31] as a basis [8, 43]. Missing parameters were

obtained from a previous study [8] and via torsion scans of two shortened molecules (see Online Resource 1 for details).

For the study of spontaneous binding of dissolved bile acids to the TMD of BASIC, eight bile acids were placed into the solvent at a distance of approx. 2 nm to the membrane of the reference system described above. This system was simulated for 1 ns with position restraints on the protein and the bile acids to allow for an equilibration of the surrounding water molecules.

The number of lipid molecules in protein docked t-DCA systems was equivalent to the reference starting structure; however, one lipid was removed in the upper layer of docking model 3 (see Online Resource 1) due to steric overlaps with t-DCA. Each protein docked t-DCA system was energy minimized using the steepest descent algorithm (2000 steps) and simulated for 2 ns using position restraints on protein backbone atoms and t-DCA heavy atoms.

Simulation conditions

MD simulations were conducted in GROMACS 5.0.x [34] using the Amber 14SB force field [7] in conjunction with Lipid14 [14] with similar simulation conditions as described previously [36]. In short, the temperature was kept constant at 310 K with a time constant of 0.5 ps and the v-rescale temperature coupling scheme [6]. Further, a semi-isotropic pressure of 1 bar was maintained with the Berendsen barostat [4] using a time constant of 1 ps. Long-range electrostatic interactions were calculated using particle-mesh Ewald summation [9] with a real-space cutoff of 1.0 nm; van der Waals interactions were treated with a Verlet cutoff scheme [33] with $r_{vdw} = 1.0$ nm. The integration time step was chosen to 2 fs, and the solvent was described with the TIP3P [44] water model. Simulations of dissolved t-DCA molecules were conducted with conditions described above in conjunction with the ILDN refinement [30]. Simulations with dissolved bile acids (one system) and docked BASIC/t-DCA complexes (six systems) were repeated three times, summing up to in total 21 simulations (200 ns each).

Analysis

The stability of docked complexes was estimated by analyzing the root mean square deviation (rmsd) of t-DCA to its starting configuration, after fitting the system to the BASIC TMD (see Online Resource 1). Separate minimal distances were calculated between side chains A443 and D444 of human BASIC and the hydroxyl groups of t-DCA. The first 30 ns of the docking simulations were excluded from analysis for equilibration purposes.

Statistical analysis

Data are presented as mean ± SEM. Statistical significance was assessed by the appropriate version of ANOVA (with Bonferroni post hoc test) or Student's *t* test. *N* indicates the number of different batches of oocytes, and *n* indicates the number of individual oocytes studied. Statistical analysis was performed using Graph Pad Prism 5.04.

Electronic supplementary material

The Electronic Supplementary Material (Online Resource 1) contains information about the parameterization procedure of t-DCA required for the MD simulations and detailed information about docking simulations that were not described in the main text.

Results

Identification of amino acid residues critical for Ca^{2+}-mediated inhibition of human BASIC

Protein sequence alignment of the initial part of the second TMD (TMD2) of rat ASIC1 and human BASIC demonstrated a high degree of homology between these two regions (Fig. 1, 61% identity). Functional studies on rat ASIC1 have shown that two negatively charged amino acid residues (Glu 425 and Asp 432) at the beginning of TMD2 (separated by two loops of the α-helix) are involved in channel inhibition by Ca^{2+} [35]. In particular, Asp 432, which belongs to the degenerin region, is thought to be critical for ASIC1 inhibition by Ca^{2+} because its substitution by cysteine or alanine reduced the inhibitory effect of Ca^{2+} by ~90% [35]. The homologous region of BASIC also contains two negatively charged residues (Glu 440, Asp 444). Asp 444 belongs to the degenerin region and is conserved in ASIC1 and BASIC. Unlike in ASIC1, where the two negatively charged residues are separated by two α-helical loops (i.e., six amino acid residues), the residue Glu 440 in BASIC is separated from Asp 444 by only one α-helical loop (i.e., three amino acid residues). Nevertheless, the functional role of Glu 440 in BASIC may be similar to that of Glu 425 in ASIC1. We hypothesized that Asp 444 and possibly also Glu 440 are functionally relevant Ca^{2+}-binding sites in human BASIC. To test this, we substituted these negatively charged residues by non-charged alanines (D444A; E440A/D444A) and investigated the effect of extracellular Ca^{2+} removal on these mutant channels.

In *Xenopus laevis* oocytes expressing WT BASIC, washout of 100 μM diminazene, a known inhibitor of BASIC [48], revealed the expected BASIC-mediated inward current component (ΔI_{Dimi}) (Fig. 2a). Subsequent Ca^{2+} removal from the bath solution caused a reversible

Fig. 1 Putative Ca^{2+}-binding site in human BASIC. Sequence alignment of rat ASIC1 (r.ASIC) and human BASIC (h.BASIC) corresponding to the first part of the second transmembrane domain (TMD2). Negatively charged amino acid residues forming putative Ca^{2+}-binding sites are indicated in bold. The amino acid residues belonging to the degenerin region are indicated by arrows

~2.5-fold increase of the BASIC-mediated inward current consistent with the concept that the channel is partially inhibited by extracellular Ca^{2+}. Re-application of diminazene returned the stimulated inward current to the initial baseline level. Overall, these findings are consistent with previously reported data regarding the functional properties of BASIC expressed in the oocyte expression system [29, 50]. Importantly, substitution of the negatively charged aspartate residue 444 by a non-charged alanine (D444A) substantially reduced the Ca^{2+} sensitivity of BASIC (Fig. 2b). Indeed, Ca^{2+} removal only had a minor stimulatory effect on the D444A mutant channel not exceeding ~40%. The double-mutant channel E440A/D444A essentially behaved like the channel carrying the single D444A mutation (Fig. 2c). Thus, unlike the D444 residue, the E440 residue does not seem to play a major role for the Ca^{2+} sensitivity of the channel, but a minor contribution cannot be ruled out. Taken together, these findings suggest that the residue D444 is involved in Ca^{2+} inhibition of BASIC.

Interestingly, baseline currents in the presence of diminazene were significantly higher in oocytes expressing the D444A (-0.18 ± 0.02 μA, $n = 42$, $p < 0.001$) (Fig. 2b) or the E440A/D444A mutant channel (-0.20 ± 0.01 μA, $n = 51$, $p < 0.001$) (Fig. 2c) compared to those in oocytes expressing WT BASIC (-0.09 ± 0.01 μA, $n = 40$) (Fig. 2a). These findings suggest that the D444A mutation alters the sensitivity of the channel to diminazene. To investigate this further, we used a different experimental protocol with a bath solution in which Na^+ was replaced by the impermeant cation NMDG to fully block BASIC-mediated Na^+ currents (Fig. 3a, b). Switching from an NMDG bath solution to a Na^+ containing bath solution revealed BASIC-mediated Na^+ inward currents (ΔI_{NMDG}) that were inhibited by diminazene in a concentration-dependent manner. Due to limited solubility of diminazine in concentrations higher than 100 μM, an IC_{50} of diminazene-mediated BASIC inhibition could not be estimated reliably. Nevertheless, the summary data shown in Fig. 3b clearly demonstrate that the D444A mutation shifted the diminazene concentration-response curve to the right indicating that the mutation significantly reduced the sensitivity of BASIC to diminazene.

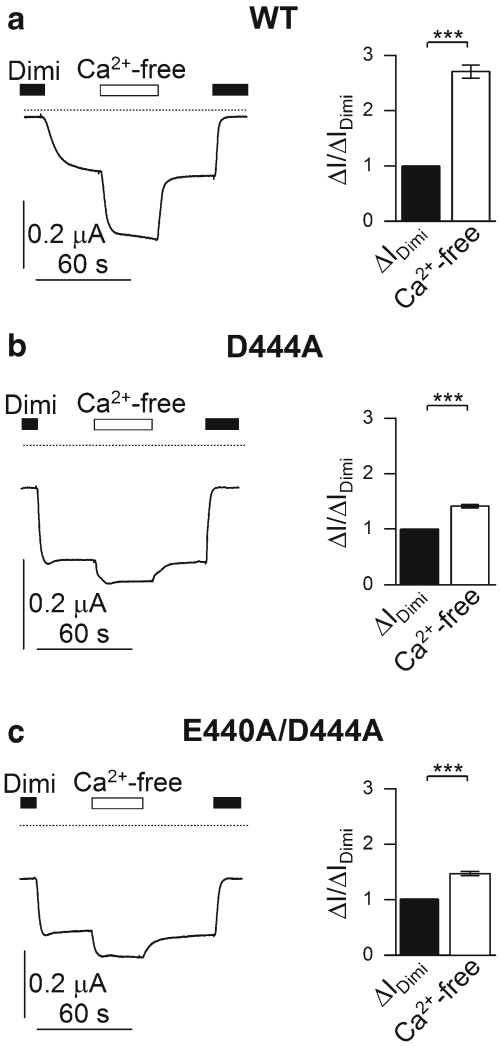

Fig. 2 Aspartate D444 in the degenerin region plays a crucial role in BASIC inhibition by Ca^{2+}. a–c Left panels: Representative whole-cell current traces recorded in oocytes expressing WT, D444A, or E440A/D444A mutant BASIC. Application of diminazene (100 μM) and removal of Ca^{2+} ions from the bath solution (Ca^{2+}-free, 1 mM EGTA) are indicated by corresponding bars. Zero current level is indicated by a dotted horizontal line. Right panels: Averaged normalized current values ($\Delta I/\Delta I_{Dimi}$) obtained from similar experiments as shown in left panels. (WT: $n = 32$, $N = 4$; D444A: $n = 36$, $N = 4$; E440A/D444A: $n = 32$, $N = 4$). The baseline current in the presence of diminazene was subtracted from the plateau current values reached after washout of diminazene (ΔI_{Dimi}) or after Ca^{2+} removal (ΔI). Mean ± SEM. ***Significantly different, $p < 0.001$; Student's t test

Identification of amino acid residues critical for bile acid-mediated activation of human BASIC

We have previously shown that the degenerin region is critically involved in the activation of human ENaC and ASIC1a by bile acids [21, 22]. Therefore, we tested whether the D444A mutation alters the stimulatory effect of the prototypical bile acid t-DCA on BASIC. Taking into consideration the different sensitivity of WT and mutant BASICs to diminazene

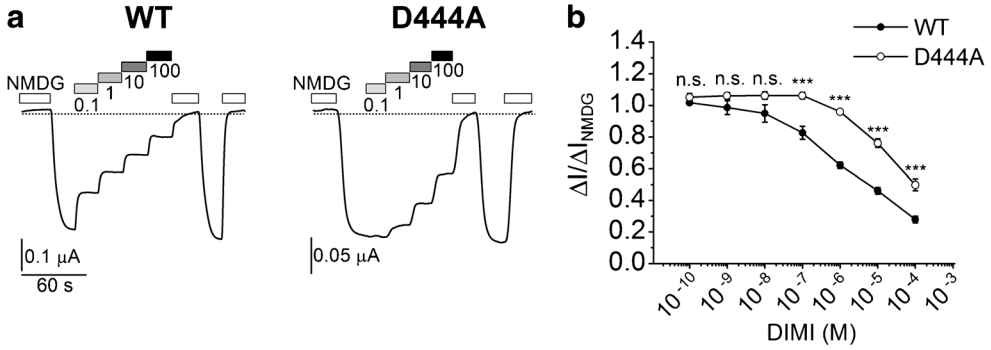

Fig. 3 D444A substitution significantly reduces BASIC affinity to diminazene. **a** Representative whole-cell current traces recorded in oocytes expressing WT or D444A mutant BASIC. Low Na^+ bath solution (NMDG) and successively increasing concentrations of diminazene (0.1, 1, 10, 100 μM) were applied as indicated by the corresponding *bars*. Zero current level is indicated by a dotted horizontal line. **b** Concentration-response curves of diminazene-dependent inhibition of BASIC currents obtained from similar recordings as shows in **a**. WT BASIC (filled circles); D444A mutant BASIC (open circles). The baseline current in the presence of NMDG was subtracted from the plateau current values reached after replacing NMDG by Na^+ in the bath solution (ΔI_{NMDG}) or after application of different concentrations of diminazene (ΔI) ($5 \leq n \leq 17$; $N = 3$). Mean ± SEM; ***Significantly different, $p < 0.001$; n.s. not significant; one-way ANOVA with Bonferroni post hoc test

and extracellular Ca^{2+}, NMDG-containing solution was used instead of diminazene to block BASIC-mediated Na^+ inward currents. Moreover, t-DCA-mediated channel stimulation was investigated under Ca^{2+}-free conditions (Fig. 4). Consistent with the results shown in Fig. 2b, the D444A mutant channel was significantly less sensitive to Ca^{2+} than the WT channel (Fig. 4a, b). In contrast, in the absence of Ca^{2+}, the sensitivity of the D444A mutant channel to t-DCA was similar to that of the WT channel (Fig. 4a, c). Recently, we have shown that the asparagine to cysteine substitution (N521C) in human βENaC, i.e., in the position homologous to D444 in BASIC, significantly reduced the stimulatory effect of bile acids on ENaC [21]. Therefore, we tested whether the cysteine substitution (D444C) in BASIC would reduce the t-DCA-mediated channel activation. Indeed, t-DCA sensitivity of the D444C mutant was significantly reduced compared to WT BASIC (Fig. 4a, c). The D444C mutant channel was also significantly less sensitive to Ca^{2+} than the WT channel (Fig. 4b). Together with D444, the alanine residue in position 443 belongs to the degenerin region of BASIC (Fig. 1). We also investigated the effect of substituting this residue by cysteine (A443C). We have previously shown that an analogous mutation in human ASIC1a (G433C) fully abolished the stimulatory effect of t-DCA on proton-activated ASIC1a currents [22]. Indeed, the A443C mutation decreased the stimulatory effect of t-DCA by about 75% (Fig. 4c). This indicates that the A443C mutation significantly reduced the bile acid sensitivity of BASIC. In contrast, the stimulatory effect of Ca^{2+} removal on the A443C mutant channel (average 1.7-fold) was only slightly reduced compared to WT BASIC (Fig. 4b). The substitution of the amino acid residue in the analogous position in human ASIC1a to serine significantly reduced the stimulatory effect of t-DCA on proton-activated ASIC1a currents [22]. Therefore, we tested whether the substitution of A443 to serine (A443S) would also reduce the t-DCA effect on BASIC (Fig. 4a). Interestingly, in contrast to the A443C mutation, A443S did not reduce the t-DCA-mediated activation (Fig. 4c) and had a relatively small effect on the Ca^{2+} sensitivity of BASIC (Fig. 4b).

Collectively, these findings highlight the critical role of D444 in Ca^{2+} inhibition and the functional importance of both A443 and D444 in bile acid-mediated stimulation of BASIC.

Extracellular Ca^{2+} has a negligible effect on t-DCA affinity to BASIC

Our finding that the neighboring amino acid residues (A443 and D444) are critically involved in t-DCA-mediated activation and Ca^{2+}-mediated inhibition of BASIC may indicate that t-DCA and Ca^{2+} compete at a common binding site in the channel pore. To explore this possibility, we investigated whether Ca^{2+} in the extracellular solution influences the concentration dependence of the stimulatory effect of t-DCA on BASIC. As shown in Fig. 5, we estimated the apparent affinity of BASIC to t-DCA in the presence and absence of Ca^{2+} in the bath solution. t-DCA was applied in different concentrations in Ca^{2+}-free or in control solution containing 1 mM Ca^{2+}. The highest t-DCA concentration applied was 500 μM as prolonged exposure of oocytes to t-DCA in a concentration higher than 500 μM is likely to compromise the integrity of their plasma membrane. Due to this limitation, it was not feasible to determine the EC_{50} of the t-DCA-mediated BASIC stimulation. Nevertheless, the experiments indicate that the relative stimulatory effect of t-DCA was similar in the presence or absence of Ca^{2+} in the bath solution (Fig. 5a, b). The subtle difference at 500 μM t-DCA cannot be taken as evidence that Ca^{2+} affects the affinity of t-DCA to BASIC. This finding demonstrates that both maneuvers, t-DCA and Ca^{2+} removal, stimulate BASIC by independent molecular mechanisms. Next, we attempted to elucidate these

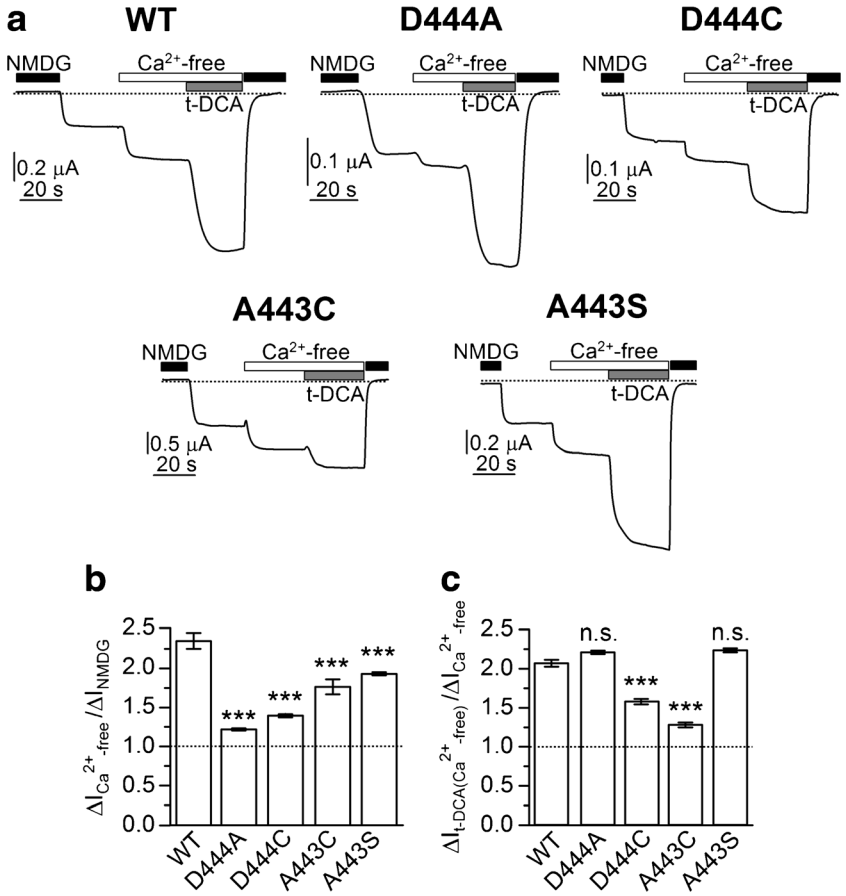

Fig. 4 Comparison of the stimulatory effects of Ca^{2+}-removal and t-DCA application in WT, D444A, D444C, A443C or A443S mutant BASIC. **a** Representative whole-cell current traces recorded in oocytes expressing WT, D444A, D444C, A443C, or A443S mutant BASIC. Low Na^+ solution (NMDG), tauro-deoxycholic acid (t-DCA, 500 μM), and Ca^{2+}-free solution (Ca^{2+}-free, 1 mM EGTA) are indicated by corresponding bars. Zero current level is indicated by a dotted horizontal line. **b** Averaged normalized current values upon Ca^{2+} removal ($\Delta I_{Ca^{2+}\text{-free}}/\Delta I_{NMDG}$) from similar experiments as shown in **a**. The baseline current in the presence of NMDG was subtracted from the plateau current values reached after replacing NMDG by Na^+ in the bath solution (ΔI_{NMDG}) or after Ca^{2+} removal ($\Delta I_{Ca^{2+}\text{-free}}$). **c** Averaged normalized current values upon t-DCA application under Ca^{2+}-free conditions ($\Delta I_{\text{t-DCA }(Ca^{2+}\text{-free})}/\Delta I_{Ca^{2+}\text{-free}}$) obtained from similar experiments as shown in **a**. The baseline current in the presence of NMDG was subtracted from the plateau current values reached after Ca^{2+} removal ($\Delta I_{Ca^{2+}\text{-free}}$) or after Ca^{2+} removal in the presence of t-DCA ($\Delta I_{\text{t-DCA }(Ca^{2+}\text{-free})}$). WT: $n = 18$, $N = 3$; D444A: $n = 17$, $N = 3$; D444C: $n = 32$, $N = 2$; A443C: $n = 21$, $N = 3$; A443S: $n = 22$, $N = 2$. Mean ± SEM. ***Significantly different, $p < 0.001$; n.s. not significant; one-way ANOVA with Bonferroni post hoc test

mechanisms using computer simulations and single-channel recordings.

Computer simulations suggest that t-DCA may interact with the degenerin region in the open state of BASIC

The experimental data suggest that D444 is critically involved in BASIC inhibition by Ca^{2+}, whereas both D444 and A443 are involved in t-DCA-mediated channel stimulation. The BASIC homology models in closed and open states show a huge difference in the opening of the outer vestibule of the channel: In the closed state, the D444 residues are found at a distance of 5.3 Å, while the channel entrance is widened to approximately 13 Å in the open state (Fig. 6). These findings suggest that Ca^{2+} may bind to two or three aspartic acids (D444) of the degenerin region simultaneously, thereby inhibiting BASIC opening by stabilizing the closed state of the channel. In turn, A443 is inaccessible to t-DCA in the closed state. Accordingly, we used the open channel conformation for t-DCA docking and MD simulations.

To explore whether t-DCA can directly bind to the degenerin region, we investigated the spontaneous interaction of dissolved t-DCA molecules with the lipid bilayer and the TMDs of BASIC using atomistic MD simulations. To this end, we generated a homology model of the human BASIC TMD based on the crystal structure of chicken ASIC1 in open conformation (PDB #4NTW [3]). The TMD were embedded into a POPC bilayer, and three 200-ns-long simulations were performed. t-DCA molecules were initially placed into the solvent at a distance of approximately 2 nm to the membrane. In all simulations, t-DCA molecules formed clusters of up to

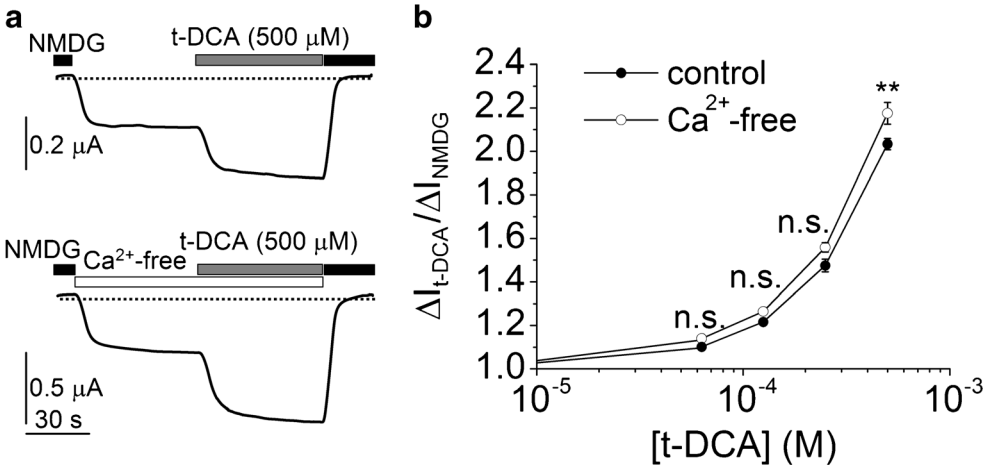

Fig. 5 Concentration-dependent stimulation of WT BASIC by t-DCA in the presence and absence of Ca^{2+} in the bath solution. **a** Representative whole-cell current traces recorded in oocytes expressing WT BASIC. Low Na^+ solution (NMDG), tauro-deoxycholic acid (t-DCA, 500 μM), and Ca^{2+}-free solution (Ca^{2+}-free, 1 mM EGTA) are indicated by corresponding bars. Zero current level is indicated by a dotted horizontal line. **b** Concentration-response curve of t-DCA-dependent stimulation of BASIC currents recorded in the presence of Ca^{2+} in the bath solution (1 mM, control, filled circles) or in its absence (1 mM EGTA, Ca^{2+}-free, open circles). t-DCA was applied at different concentrations in similar experiments as shown in **a**. The baseline current in the presence of NMDG was subtracted from the plateau current values reached after replacing NMDG by Na^+ in Ca^{2+}-containing or Ca^{2+}-free bath solution (ΔI_{NMDG}) or after t-DCA application ($\Delta I_{t\text{-}DCA}$) ($n = 15$; $N = 3$). Mean ± SEM. **Significantly different, $p < 0.01$; n.s. not significant; one-way ANOVA with Bonferroni post hoc test

four molecules or remained in the monomeric state, and attached transiently and recurrently to BASIC while interacting predominately with lysines at position 434 located at the extracellular site of the TMD2 helices (Fig. 7a, b). This position may, however, not be accessible within the full untruncated channel. Individual t-DCA molecules also absorbed to the membrane-water interface region by establishing hydrogen bonds to headgroups of membrane lipids. Absorbed t-DCA molecules were also observed to diffuse towards BASIC and interact with its TMD (Fig. 7a, b). Importantly, we observed the spontaneous translocation of a t-DCA molecule from the water phase to the outer vestibule of the channel pore where it formed a hydrogen bond with D444 (Fig. 7c).

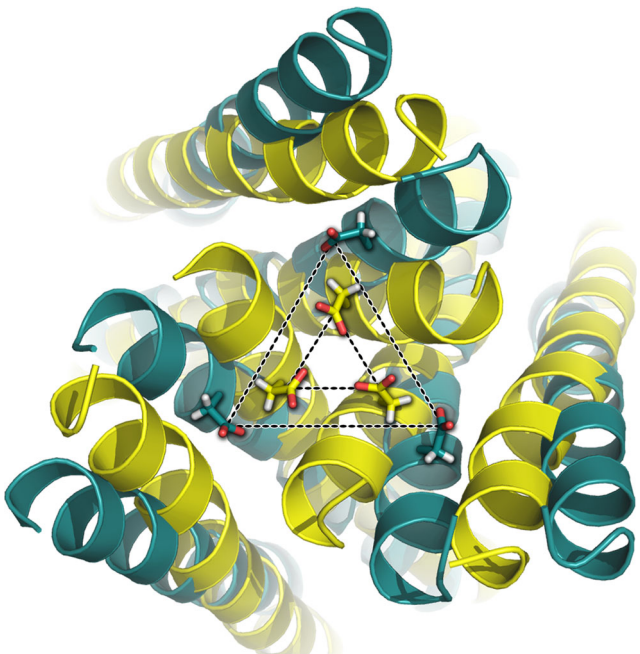

Fig. 6 Overlay of the open and closed states of the BASIC TMD. The homology model of the open state is shown in cyan; the closed state is represented in yellow. As a reference for the outer vestibule size, the D444 residues of all subunits are shown as sticks and connected with dashed lines. The distances between D444 are ~ 5.3 Å in the closed state and ~ 13 Å in the open state

These data suggest that t-DCA may interact spontaneously with the TMD of BASIC. To explore this further, a molecular docking approach was used [45] in combination with atomistic MD simulations. From molecular docking simulations, we selected six representative docking models of t-DCA bound to the pore region of BASIC (see Online Resource 1, Fig. S1, S2). These docked complexes were investigated in lipid environment using three 200-ns-long atomistic MD simulations for each docking model (i.e., 18 simulations in total). The relative root mean square deviation (rmsd) of bound t-DCA from its initial docked configuration was calculated to estimate the stability of t-DCA binding (see Online Resource 1, Fig. S3). Three of the studied models showed moderate positional changes of t-DCA in the range of approximately 0.5–1 nm. Temporary unbinding was observed in only 2 of the 18 simulations. However, a single stable binding configuration of t-DCA could not be identified. Examples of typical metastable binding configurations are shown in Fig. 8. In its initial configuration (see Online Resource 1, Fig. S2, model 6), t-DCA points with its sulfur group towards the extracellular side and faces BASIC with its two hydroxyl groups. During the

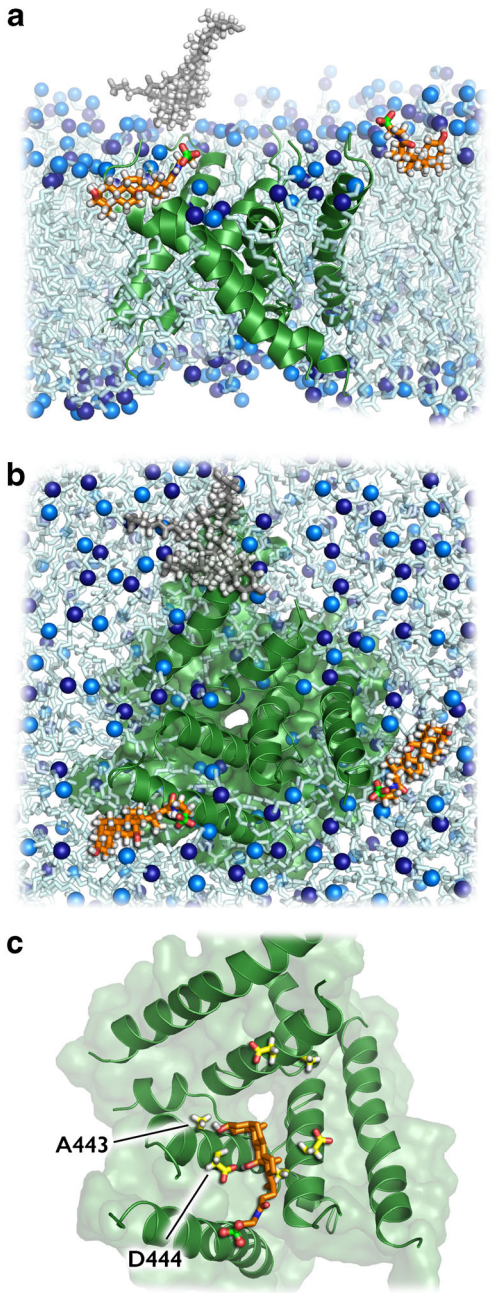

Fig. 7 Spontaneous binding of t-DCA to the lipid bilayer and transmembrane domains of BASIC. Side view (**a**) and top view (**b**) of a spontaneous binding simulation (sim. 3, $t = 200$ ns) showing two individual membrane bound bile acids that approached the protein and a cluster of four t-DCA molecules interacting with the TMD of BASIC from the solvent. The latter binding mode (shaded in gray) is likely enabled due to the absence of the large extracellular domain in the simulations. **c** A t-DCA molecule spontaneously inserted into the inter-subunit space of BASIC to form a hydrogen bond with D444 via its hydroxyl group (sim. 2, $t =$ 130 ns). The protein is shown in green cartoon representation, and A443/D444 of each subunit are shown in yellow sticks. t-DCA molecules are colored in orange with sulfur in green, oxygen in red, and hydrogens in white. The membrane is colored in blue tones. For clarity, the membrane and hydrogen atoms of t-DCA are hidden in **c**

performed simulations, t-DCA reorients in order to lie almost horizontally abreast of the outer vestibule of the channel and even temporarily occludes the channel pore (Fig. 8a, b). In these configurations, t-DCA forms h-bonds between its hydroxyl group and D444 (or E440, not shown in Fig. 8a, b) and between the sulfur group and glutamines at positions 79 and 448 in the outer vestibule of the channel pore. Interestingly, the same binding mode was observed in two independent simulations of model 4 after reorientation of the t-DCA molecule (data not shown). In a different configuration (docking pose 3, Fig. 8c), t-DCA bound between two BASIC subunits, acting thereby as an inter-subunit spacer that prevents channel closure (compare Fig. 6). Interestingly, such an inter-subunit spacer developed also within a different simulation (starting from docking pose 1, data not shown) and was reminiscent of the binding mode observed in simulations of spontaneous t-DCA binding to BASIC (Fig. 7c). Importantly, the formation of the complexes between t-DCA and BASIC shown in Fig. 8 would sterically be hindered for the closed channel state. Thus, they suggest a possible mechanism that may contribute to a t-DCA-induced stabilization of the open state of the channel.

To summarize, our docking/molecular dynamics simulations suggest that t-DCA might stabilize the open state of BASIC by binding to the outer vestibule of the channel pore or by occupying the inter-subunit space.

Single-channel analysis suggests that Ca^{2+} and t-DCA stabilize the closed and open state of BASIC, respectively

To investigate the mechanisms of BASIC activation by Ca^{2+} removal and t-DCA application at the single-channel level, outside-out patch-clamp recordings were performed. The representative continuous current trace shown in Fig. 9a was recorded from an outside-out membrane patch excised from an oocyte expressing WT BASIC. It demonstrates changes in channel activity upon diminazene washout, Ca^{2+} removal, application of t-DCA, and Ca^{2+} removal in the presence of t-DCA. In the presence of diminazene, no single-channel events could be resolved (inset 1). Washout of diminazene revealed typical basal BASIC activity characterized by rare channel openings with a current amplitude of 0.95 pA (inset 2). Removal of Ca^{2+} from the bath solution caused an abrupt shift in the baseline current level, which probably reflects a change in seal resistance and cannot be attributed to an effect on BASIC activity, because it was also observed in non-injected control oocytes [29]. Importantly, Ca^{2+} removal increased the frequency of channel openings and the single-channel current amplitude to 1.25 pA (inset 3). The effect of Ca^{2+} removal was reversible as application of the Ca^{2+}-containing solution returned BASIC activity to its basal level (inset 4). Similar to Ca^{2+} removal, application of t-DCA (500 μM) stimulated

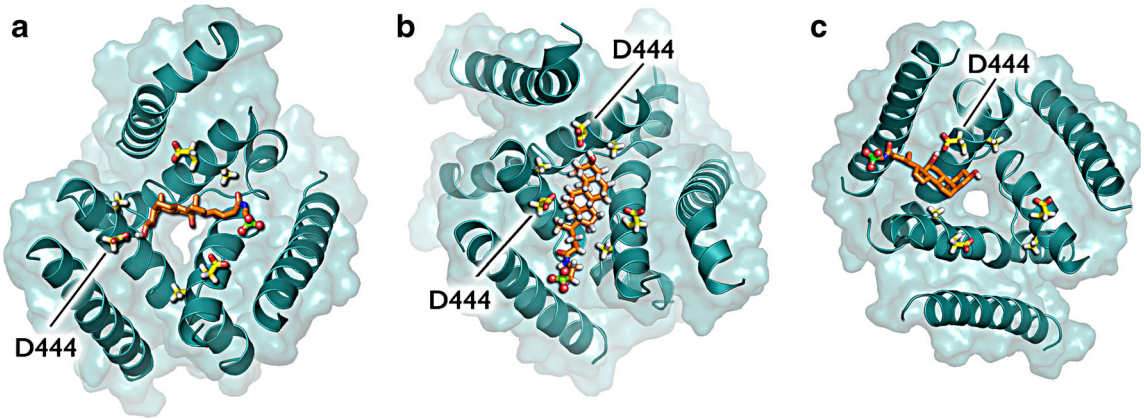

Fig. 8 t-DCA preferentially binds to the outer vestibule of the channel pore or occupies the inter-subunit space in the open state of BASIC. **a** Snapshot at $t = 60$ ns of docking model 6 simulation (sim. 1). t-DCA is stabilized by hydrogen bonds between the hydroxyl group of t-DCA and aspartate D444 in the outer vestibule of the channel. **b** Snapshot at $t = 200$ ns of the docking model 6 simulation (sim. 1). t-DCA is stabilized by hydrogen bonds between hydroxyl groups of t-DCA and aspartic acid D444. **c** Snapshot at $t = 200$ ns of docking model 3 simulation (sim. 3). t-DCA is stabilized in the inter-subunit space by a hydrogen bond between the hydroxyl group of t-DCA and D444. In **a**–**c**, A443 and D444 of each subunit are shown as yellow sticks and the membrane is hidden for clarity

BASIC activity and increased single-channel current amplitude to 1.11 pA (inset 5). Importantly, subsequent Ca^{2+} removal in the presence of t-DCA further increased channel activity as well as the single-channel current amplitude to 1.29 pA (inset 6). The calculated changes of channel activity (NP_O) and single-channel current amplitude (i) upon Ca^{2+} removal and t-DCA application are summarized in Fig. 9b, c. On average, Ca^{2+} removal or t-DCA application in Ca^{2+}-containing solution increased NP_O by about 3-fold, whereas Ca^{2+} removal in t-DCA-containing solution resulted in a more than 8-fold increase of BASIC activity in outside-out patches (Fig. 9b). These NP_O changes are in good agreement with the corresponding current changes observed in whole-cell current experiments (see Fig. 2a). A minor part of the stimulatory effect of Ca^{2+} removal or t-DCA application can be attributed to a slight but significant increase of the single-channel current amplitude from 0.95 ± 0.05 pA ($n = 7$; $N = 4$) under control conditions to 1.22 ± 0.02 pA ($n = 7$; $N = 4$) upon Ca^{2+} removal or 1.11 ± 0.01 pA ($n = 7$; $N = 4$) in the presence of t-DCA. The highest single-channel current amplitude was observed upon Ca^{2+} removal in t-DCA-containing solution (1.28 ± 0.03 pA; $n = 7$; $N = 4$; Fig. 9c). Importantly, the increase of the apparent single-channel current amplitude by both Ca^{2+} removal and t-DCA application suggests that Ca^{2+} and t-DCA interact with the pore region of BASIC. For the analysis of single-channel kinetics upon Ca^{2+} removal and t-DCA application, only patches with a single apparent channel open level were used. This does not rule out the presence of more than one channel in the selected patches. Therefore, the values reported were termed apparent mean open and apparent mean closed time (Fig. 9d, e). With Ca^{2+} removal, there was a non-significant trend for a modest increase of the apparent mean open time. A substantial and significant increase of the apparent mean open time was observed upon t-DCA application in the presence and absence of extracellular Ca^{2+} (Fig. 9d). In contrast, the apparent mean closed time appeared to be reduced more prominently by Ca^{2+} removal than by application of t-DCA in the presence of Ca^{2+} (Fig. 9e). However, in both cases, this trend was non-significant due to the considerable variability of this parameter and to the low number of recordings amenable to analysis, i.e., with only one apparent channel in the patch.

Single-channel recordings performed from outside-out patches with the double-mutant channel (E440A/D444A) demonstrated that the mutations significantly reduced the basal single-channel current amplitude (0.18 ± 0.01 pA; $n = 7$; $N = 5$; vs. 0.95 ± 0.05 pA in WT; $n = 7$; $N = 4$; $p < 0.001$; Fig. 10a, c). Ca^{2+} removal did not significantly increase NP_O of the E440A/D444A mutant channel and did not affect its single-channel current amplitude (Fig. 10b, c). Thus, these experiments confirmed that the E440A/D444A mutations substantially reduced the Ca^{2+} sensitivity of BASIC. In contrast, application of t-DCA resulted in a strong increase of NP_O by about 2.5-fold and produced a substantial increase of the single-channel current amplitude to 0.24 ± 0.02 pA ($n = 7$; $N = 5$). These findings suggest that t-DCA but not Ca^{2+} interact with the channel pore of the E440A/D444A mutant channel. Analysis of single-channel kinetics demonstrated that only t-DCA application, but not Ca^{2+}-removal, significantly increased the apparent mean open time of the E440A/D444A mutant channel (Fig. 10d). Under control conditions, the basal apparent mean closed time of the mutant channel (Fig. 10e) appeared to be slightly reduced compared to WT BASIC and was not affected by Ca^{2+} removal or t-DCA application (Fig. 10e).

Next, we studied the effects of Ca^{2+} removal and t-DCA application on the A443C mutant BASIC at the single-channel level (Fig. 11a). Our data demonstrate that the A443C mutation did not affect the basal single-channel

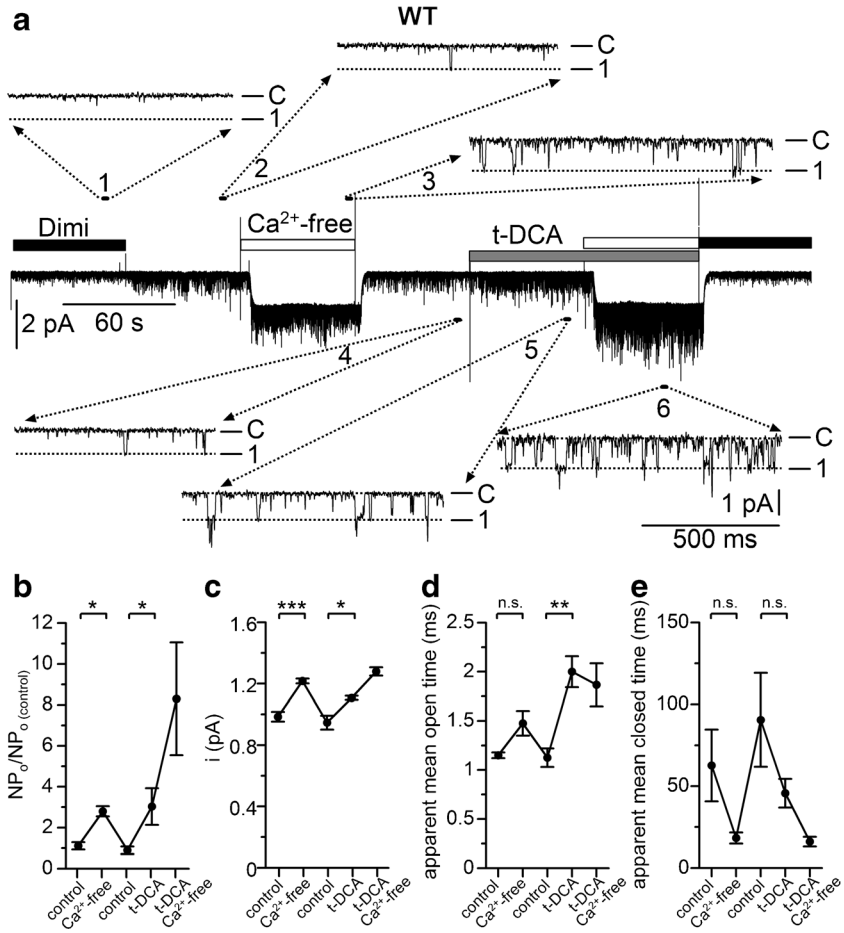

Fig. 9 Ca^{2+} removal as well as t-DCA application increases the activity of WT BASIC in single-channel recordings. **a** Representative continuous single-channel current recording in an outside-out patch of a WT BASIC expressing oocyte obtained at a holding potential of − 70 mV. Application of diminazene (10 μM), tauro-deoxycholic acid (t-DCA, 500 μM), and removal of Ca^{2+} ions from the bath solution (Ca^{2+}-free, 1 mM EGTA) are indicated by corresponding bars. The insets (1–6) show the indicated fragments of the current trace on an extended timescale. The current level at which all channels are closed (C) was determined in the presence of diminazene. The channel open level is indicated by (1). Single-channel binned current amplitude histograms were obtained by analyzing a 60-s portion of the current trace for each experimental condition (control, Ca^{2+}-free, Ca^{2+} reapplication, t-DCA, t-DCA/Ca^{2+}-free) and were used to calculate NP_O values and single-channel current amplitude (*i*). **b** Average *NPo* data from similar experiments as shown in **a**. In each experiment, NP_O values after diminazene washout (control), Ca^{2+} removal (Ca^{2+}-free), Ca^{2+} reapplication (control), t-DCA application in the presence of Ca^{2+} (t-DCA), or t-DCA application in the absence of Ca^{2+} (t-DCA/Ca^{2+}-free) were normalized to the mean NP_O obtained after diminazene washout and Ca^{2+} reapplication ($NP_{O(\text{control})}$) in the same experiment. **c** Averaged single-channel current amplitude values (*i*) from similar experiments as shown in **a** after diminazene washout (control), Ca^{2+} removal (Ca^{2+}-free), Ca^{2+} reapplication (control), t-DCA application in the presence of Ca^{2+} (t-DCA), or t-DCA application in the absence of Ca^{2+} (t-DCA/Ca^{2+}-free) (mean ± SEM; $n = 7$; $N = 4$; ***, *Significantly different, $p < 0.001$, $p < 0.05$, respectively; n.s. not significant; one-way repeated measures ANOVA with Bonferroni post hoc test). **d**, **e** Averaged apparent mean open (**d**) and closed (**e**) time of the channel after diminazene washout (control), Ca^{2+} removal (Ca^{2+}-free), Ca^{2+} reapplication (control), t-DCA application in the presence of Ca^{2+} (t-DCA), or application of t-DCA in the absence of Ca^{2+} (t-DCA/Ca^{2+}-free) obtained from recordings with only one open channel level in the patch. Mean ± SEM; $n = 4$; $N = 3$. **Significantly different, $p < 0.01$; n.s. not significant; one-way repeated measures ANOVA with Bonferroni post hoc test

current amplitude (0.93 ± 0.03 pA, $n = 9$, $N = 4$ in A443C vs. 0.95 ± 0.05 pA, $n = 7$; $N = 4$ in WT; n.s.). Importantly, t-DCA application neither significantly increased NP_O nor single-channel current amplitude (Fig. 11b, c) indicating that the A443C mutation prevented the interaction of t-DCA with the channel pore. Analysis of single-channel kinetics further supported this conclusion, as the effect of t-DCA on the apparent mean open time was blunted compared to WT and E440A/D444A mutant BASIC (Fig. 11d). In contrast, Ca^{2+} removal significantly increased both NP_O and the single-channel current amplitude and showed a non-significant trend to reduce the apparent mean closed time. These findings indicate that the Ca^{2+} sensitivity of the A443C mutant channel remained largely unchanged.

Collectively, our single-channel recordings suggest that Ca^{2+}-mediated BASIC inhibition can be attributed mainly to stabilization of the closed state of the channel. In contrast, t-DCA activates BASIC by stabilizing the open state of the channel.

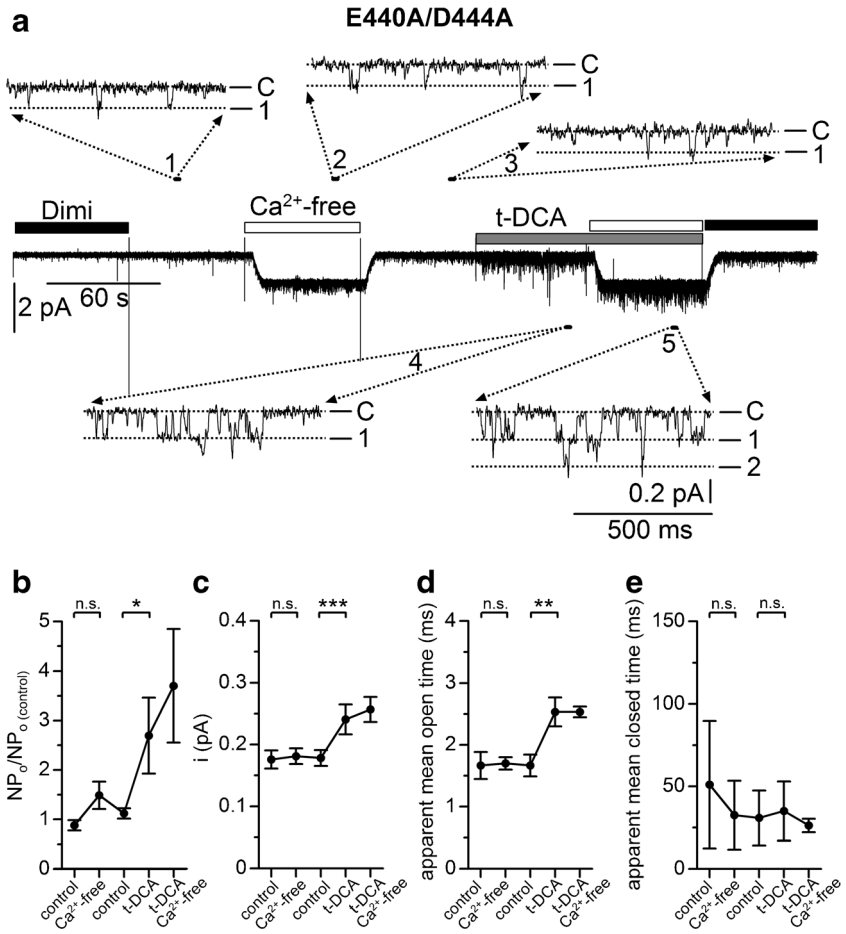

Fig. 10 Ca^{2+} removal did not significantly increase the activity of E440A/D444A mutant BASIC in single-channel recordings. **a** Representative continuous single-channel current recording in an outside-out patch of an E440A/D444A mutant BASIC expressing oocyte recorded and analyzed essentially as described in Fig. 9a. **b**, **c** Summary of data from similar experiments as shown in **a** (mean ± SEM; $n = 7$; $N = 5$; ***, *Significantly different, $p < 0.001$, $p < 0.05$, respectively; n.s. not significant; one-way repeated measures ANOVA with Bonferroni post hoc test). **d**, **e** Analysis of single-channel kinetics from recordings with only one open channel level in the patch (mean ± SEM; $n = 3$; $N = 2$; **Significantly different, $p < 0.01$; n.s. not significant; one-way repeated measures ANOVA with Bonferroni post hoc test)

Discussion

In this study, we demonstrated the functional importance of the degenerin region in mediating the inhibition of BASIC by Ca^{2+} and its activation by t-DCA. Moreover, the combination of single-channel patch-clamp measurements with MD simulations revealed possible molecular mechanisms for Ca^{2+}-mediated BASIC inhibition and t-DCA-mediated stimulation of BASIC activity.

Possible mechanism for Ca^{2+}-mediated BASIC inhibition

The functional importance of the degenerin region in Ca^{2+}-mediated BASIC inhibition is supported by the observation that both D444A and D444C mutations significantly reduced the stimulatory effect of Ca^{2+} removal on BASIC. The significant reduction of the single-channel current amplitude in the presence of Ca^{2+} observed in patch-clamp recordings of WT BASIC further supports the hypothesis that Ca^{2+} interacts with the pore region of the channel. Importantly, the single-channel current amplitude in rat ASIC1 was also reduced by extracellular Ca^{2+}, and the homologous aspartate 432 played a critical role in Ca^{2+} sensitivity of ASIC1 [35]. Recently, it has been shown that removal of negative charge at the homologous position (D556) disrupts Ca^{2+} sensitivity of FMRFamide-gated Na^+ channel (FaNaC), another member of ENaC/degenerin family of ion channels [15]. The conclusion that Ca^{2+} binding stabilizes the closed state of the channel is supported by the observation that in patch-clamp recordings, Ca^{2+} removal was associated with a reversible decrease of the mean closed time of WT BASIC. Moreover, for the E440A/D444A mutant with reduced Ca^{2+} sensitivity, the basal mean closed time in the presence of Ca^{2+} was reduced compared to WT BASIC and was not changed upon Ca^{2+} removal or reapplication. The comparison of the BASIC models in open and closed state further supports the conclusion that Ca^{2+} binding to D444 may stabilize the closed state of the channel. In the closed state of BASIC, three negatively charged D444 residues are close enough to each other (~ 5.3 Å) to allow an interaction with Ca^{2+} which may prevent the opening of the channel. In contrast, in the open state, the outer vestibule of the channel widens and the distance between D444 residues increases up to ~ 13 Å. Consequently, the coordination of Ca^{2+} by D444 residues is prevented. Moreover, analysis of the chicken ASIC1 crystal structure in

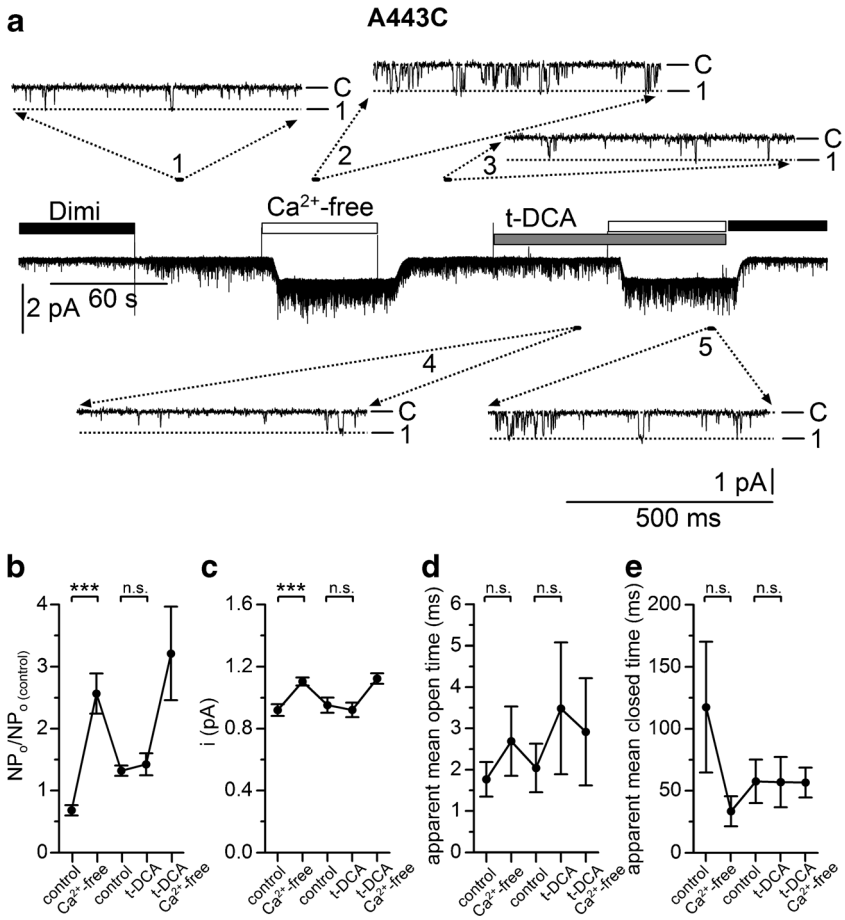

Fig. 11 Application of t-DCA did not significantly increase the activity of A443C mutant BASIC in single-channel recordings. **a** Representative continuous single-channel current recording in an outside-out patch of an A443C mutant BASIC expressing oocyte recorded and analyzed essentially as described in Fig. 9a. **b**, **c** Summary of data from similar experiments as shown in **a** (mean ± SEM; $n = 9$; $N = 4$; ***Significantly different, $p < 0.001$; n.s. not significant; one-way repeated measures ANOVA with Bonferroni post hoc test). **d**, **e** Analysis of single-channel kinetics from recordings with only one open channel level in the patch (mean ± SEM; $n = 4$; $N = 3$; n.s. not significant; one-way repeated measures ANOVA with Bonferroni post hoc test)

the desensitized state suggests that monovalent or divalent (Ca^{2+} or Mg^{2+}) cations may be bound to aspartates 433, the residues homologous to D444 in human BASIC [16]. Thus, BASIC and ASIC1 exhibit similarities in the mechanism of Ca^{2+}-mediated channel inhibition.

To conclude, Ca^{2+} may inhibit BASIC by interacting with negatively charged aspartates D444 in the outer vestibule of the channel pore, thereby stabilizing the closed state of the channel.

Possible mechanism for t-DCA-mediated BASIC activation

Our findings suggest that t-DCA stimulates BASIC and stabilizes the channel open state, probably by interacting with D444 and/or A443, i.e., residues forming the degenerin region of the channel.

The functional importance of the degenerin region in t-DCA-mediated BASIC activation is supported by the observation that D444C and A443C mutations significantly reduced the stimulatory effect of t-DCA application on BASIC. The degenerin site is critically involved in channel gating of ENaC/DEG channels. The introduction of bulky side chains to degenerin sites in these channels results in hyperactivity of the mutant channels [26]. In particular, mutation of the degenerin position in BASIC to a bulky amino acid leads to the formation of hyperactive channels [38]. Bile acids are naturally occurring ligands that may interact with the degenerin region of BASIC and increase its activity mimicking the effect of bulky mutations. This finding is in a good agreement with our previous observations that the degenerin region plays a critical role in the activation of human ENaC and ASIC1a by bile acids [21, 22]. The hypothesis that t-DCA may interact with the channel pore was further supported by our observation that application of t-DCA significantly increases the single-channel current amplitude in patch-clamp recordings. Interestingly, in human ENaC and ASIC1a, the stimulation of channel activity by bile acids was associated with a decrease of the single-channel current amplitude [21, 22]. The precise mechanism of bile acid effects on the single-channel current amplitude as well as the reason for the differences between the different ENaC/DEG channels remains to be elucidated.

The conclusion that t-DCA stabilizes the open state of the channel is supported by the fact that in patch-clamp recordings, application of t-DCA increased the mean open time of the channel. The hypothesis that t-DCA interacts with the degenerin region of BASIC only in the open state of the

channel is in good agreement with our previous observations that "near-silent" ENaC channels (channels that reside in closed state almost all the time) are insensitive to t-DCA [21] and that t-DCA potentiated ASIC1a only when the channel was opened by protons [22].

Our computer simulations suggest two most likely additive mechanisms that may result in a t-DCA-mediated stabilization of BASIC in its open state. First, bile acids may stabilize the open conformation due to steric reasons. Binding of t-DCA to the outer vestibule of the channel pore allows t-DCA to form hydrogen bonds with several amino acid residues including the aspartic acids in position 444 of the degenerin region via its hydroxyl or SO_3 groups. Despite the fact that t-DCA may also (temporarily) occlude the channel pore, t-DCA binds to BASIC only weakly, which allows for an easy reorientation of t-DCA and does not prevent the passage of Na^+ ions through the channel. Alternatively, t-DCA may occupy the inter-subunit space of BASIC where it interacts with different residues including D444. This configuration permits improved channel access for cation passage since t-DCA is not occluding the pore. t-DCA was stabilized in the inter-subunit space not only by its interaction with BASIC but also by interactions with the membrane. Importantly, the binding of t-DCA neither to the channel outer vestibule nor to the inter-subunit space would be feasible in the closed state. Interestingly, no global t-DCA binding site could be identified using the combined docking/simulation approach. Rather, t-DCA binds flexibly to BASIC by temporarily forming hydrogen bonds with several amino acid residues of the channel. This may explain why neither D444C nor A443C fully abolished the effect of t-DCA on BASIC. Our computer simulations demonstrated a preference of t-DCA for D444 over A443. Thus, the decreased sensitivity of A443C mutant to t-DCA may be explained not only by the disturbed interaction of t-DCA with the amino acid residue at the position 443 but also by the slight conformational change of the outer vestibule of BASIC introduced by the cysteine mutation, which prevents the bile acid interaction with the inter-subunit space and/or outer vestibule of BASIC.

Second, being surface-active substances, bile acids may modulate the membrane environment of BASIC. In our simulations of spontaneous interaction of dissolved t-DCA with the lipid bilayer and TMDs of BASIC, t-DCA molecules were observed to bind to the membrane interface. Membrane-embedded t-DCA molecules likely induce membrane stress resulting in a positive spontaneous membrane curvature, which in turn may be sensed by BASIC. Indeed, Schmidt et al. recently demonstrated that surface-active molecules other than bile acids activate rat and mouse BASIC [41]. This supports the hypothesis that bile acids may activate BASIC also via alteration of its membrane lipid environment. The notion that BASIC function may be affected by membrane properties was further supported by the identification of the membrane-interacting amphiphilic α-helical structure within the N-terminal domain of BASIC [42]. However, the truncation of this domain did not prevent but even increased the stimulatory effect of bile acids on BASIC indicating that this domain is not responsible for BASIC bile-acid sensitivity. Thus, the degenerin region is the only bile acid sensing site identified so far. To summarize, we cannot exclude the possibility that a modulation of membrane characteristics may contribute to the t-DCA-mediated stimulation. However, this possibility does not argue against a functional importance of the degenerin region in mediating a t-DCA effect on BASIC.

In conclusion, our results highlight the potential role of the degenerin region as a regulatory site involved in the functional interaction of Ca^{2+} and t-DCA with human BASIC.

Acknowledgements The expert technical assistance of Ralf Rinke is gratefully acknowledged. This work was supported by grants of the Deutsche Forschungsgemeinschaft (DFG) (HA 6655/1-1 to S.H.), the DFG Research Training Group 1962/1, *Dynamic Interactions at Biological Membranes—From Single Molecules to Tissue* (S.A.K. and R.A.B.), and the Johannes and Frieda Marohn Stiftung (C.K.). Part of this work has been published in abstract form [20]. We thank Kristyna Pluhackova for support in the parameterization procedure.

Abbreviations *BASIC*, Bile acid-sensitive ion channel; *ENaC*, Epithelial sodium channel; *ASIC1*, Acid-sensing ion channel 1; P_o, Open probability; *t-DCA*, Tauro-deoxycholic acid; *TMD*, Transmembrane domain

Author contributions Alexandr V. Ilyaskin, Alexei Diakov, and Sonja A. Kirsch performed the experiments, analyzed the data, and prepared the figures (Alexandr V. Ilyaskin, Alexei Diakov: electrophysiological experiments; Alexandr V. Ilyaskin: molecular docking simulations; Sonja A. Kirsch: molecular dynamics simulations). Alexandr V. Ilyaskin, Sonja A. Kirsch, Rainer A. Böckmann, Heinrich Sticht, Christoph Korbmacher, Silke Haerteis, and Alexei Diakov designed the study, interpreted the data, and wrote the paper. All authors approved the final version of the manuscript.

Compliance with ethical standards

Conflict of interest The authors declare that they have no conflict of interest.

References

1. Arnold K, Bordoli L, Kopp J, Schwede T (2006) The SWISS-MODEL workspace: a web-based environment for protein structure homology modelling. Bioinformatics 22:195–201. https://doi.org/10.1093/bioinformatics/bti770
2. Baconguis I, Gouaux E (2012) Structural plasticity and dynamic selectivity of acid-sensing ion channel-spider toxin complexes. Nature 489:400–405. https://doi.org/10.1038/nature11375
3. Baconguis I, Bohlen CJ, Goehring A, Julius D, Gouaux E (2014) X-ray structure of acid-sensing ion channel 1-snake toxin complex reveals open state of a Na^+-selective channel. Cell 156:717–729. https://doi.org/10.1016/j.cell.2014.01.011
4. Berendsen H, Postma J, van Gunsteren W, DiNola A, Haak JR (1984) Molecular dynamics with coupling to an external bath. J Chem Phys 81:3684–3690. https://doi.org/10.1063/1.448118

5. Biasini M, Bienert S, Waterhouse A, Arnold K, Studer G, Schmidt T, Kiefer F, Gallo Cassarino T, Bertoni M, Bordoli L, Schwede T (2014) SWISS-MODEL: modelling protein tertiary and quaternary structure using evolutionary information. Nucleic Acids Res 42: W252–W258. https://doi.org/10.1093/nar/gku340
6. Bussi G, Donadio D, Parrinello M (2007) Canonical sampling through velocity rescaling. J Chem Phys 126:014101. https://doi.org/10.1063/1.2408420
7. Case D, Babin V, Berryman J et al. (2014) Amber 14. University of California
8. Chen X, Minofar B, Jungwirth P, Allen HC (2010) Interfacial molecular organization at aqueous solution surfaces of atmospherically relevant dimethyl sulfoxide and methanesulfonic acid using sum frequency spectroscopy and molecular dynamics simulation. J Phys Chem B 114:15546–15553. https://doi.org/10.1021/jp1078339
9. Darden T, York D, Pedersen L (1993) Particle mesh Ewald: an N · log (N) method for Ewald sums in large systems. J Chem Phys 98: 10089–10092. https://doi.org/10.1063/1.464397
10. Dawson RJ, Benz J, Stohler P, Tetaz T, Joseph C, Huber S, Schmid G, Hugin D, Pflimlin P, Trube G, Rudolph MG, Hennig M, Ruf A (2012) Structure of the acid-sensing ion channel 1 in complex with the gating modifier Psalmotoxin 1. Nat Commun 3:936. https://doi.org/10.1038/ncomms1917
11. Diakov A, Korbmacher C (2004) A novel pathway of ENaC activation involves an SGK1 consensus motif in the C-terminus of the channel's α-subunit. J Biol Chem 279:38134–38142. https://doi.org/10.1074/jbc.M403260200
12. Diakov A, Bera K, Mokrushina M, Krueger B, Korbmacher C (2008) Cleavage in the γ-subunit of the epithelial sodium channel (ENaC) plays an important role in the proteolytic activation of near-silent channels. J Physiol 586:4587–4608. https://doi.org/10.1113/jphysiol.2008.154435
13. Diakov A, Nesterov V, Mokrushina M, Rauh R, Korbmacher C (2010) Protein kinase B alpha (PKBalpha) stimulates the epithelial sodium channel (ENaC) heterologously expressed in Xenopus laevis oocytes by two distinct mechanisms. Cell Physiol Biochem 26:913–924. https://doi.org/10.1159/000324000
14. Dickson CJ, Madej BD, Skjevik AA, Betz RM, Teigen K, Gould IR, Walker RC (2014) Lipid14: the amber lipid force field. J Chem Theory Comput 10:865–879. https://doi.org/10.1021/ct4010307
15. Fujimoto A, Kodani Y, Furukawa Y (2017) Modulation of the FMRFamide-gated Na^+ channel by external Ca^{2+}. Arch Eur J Physiol 469:1335–1347. https://doi.org/10.1007/s00424-017-2021-z
16. Gonzales EB, Kawate T, Gouaux E (2009) Pore architecture and ion sites in acid-sensing ion channels and P2X receptors. Nature 460: 599–604. https://doi.org/10.1038/nature08218
17. Guex N, Peitsch MC, Schwede T (2009) Automated comparative protein structure modeling with SWISS-MODEL and Swiss-PdbViewer: a historical perspective. Electrophoresis 30 Suppl 1: S162–S173. https://doi.org/10.1002/elps.200900140
18. Haerteis S, Krueger B, Korbmacher C, Rauh R (2009) The δ-subunit of the epithelial sodium channel (ENaC) enhances channel activity and alters proteolytic ENaC activation. J Biol Chem 284: 29024–29040. https://doi.org/10.1074/jbc.M109.018945
19. Haerteis S, Krappitz A, Krappitz M, Murphy JE, Bertog M, Krueger B, Nacken R, Chung H, Hollenberg MD, Knecht W, Bunnett NW, Korbmacher C (2014) Proteolytic activation of the human epithelial sodium channel by trypsin IV and trypsin I involves distinct cleavage sites. J Biol Chem 289:19067–19078. https://doi.org/10.1074/jbc.M113.538470
20. Ilyaskin A, Diakov A, Sticht H, Korbmacher C, Haerteis S (2016) The degenerin region of the human bile acid sensitive ion channel is involved in channel inhibition by calcium and activation by bile acids. Acta Physiol 216(S707):70–84. https://doi.org/10.1111/apha.12671
21. Ilyaskin AV, Diakov A, Korbmacher C, Haerteis S (2016) Activation of the human epithelial sodium channel (ENaC) by bile acids involves the degenerin site. J Biol Chem 291:19835–19847. https://doi.org/10.1074/jbc.M116.726471
22. Ilyaskin AV, Diakov A, Korbmacher C, Haerteis S (2017) Bile acids potentiate proton-activated currents in Xenopus laevis oocytes expressing human acid-sensing ion channel (ASIC1a). Physiol Rep 5: e13132. https://doi.org/10.14814/phy2.13132
23. Irwin JJ, Shoichet BK (2005) ZINC-a free database of commercially available compounds for virtual screening. J Chem Inf Model 45: 177–182. https://doi.org/10.1021/ci049714+
24. Jasti J, Furukawa H, Gonzales EB, Gouaux E (2007) Structure of acid-sensing ion channel 1 at 1.9 A resolution and low pH. Nature 449:316–323
25. de Jong DH, Singh G, Bennett WF, Arnarez C, Wassenaar TA, Schäfer LV, Periole X, Tieleman DP, Marrink SJ (2013) Improved parameters for the Martini coarse-grained protein force field. J Chem Theory Comput 9:687–697. https://doi.org/10.1021/ct300646g
26. Kellenberger S, Schild L (2015) International Union of Basic and Clinical Pharmacology. XCI. Structure, function, and pharmacology of acid-sensing ion channels and the epithelial Na^+ channel. Pharmacol Rev 67:1–35. https://doi.org/10.1124/pr.114.009225
27. Kiefer F, Arnold K, Kunzli M, Bordoli L, Schwede T (2009) The SWISS-MODEL repository and associated resources. Nucleic Acids Res 37:D387–D392. https://doi.org/10.1093/nar/gkn750
28. Korbmacher C, Volk T, Segal AS, Boulpaep EL, Frömter E (1995) A calcium-activated and nucleotide-sensitive nonselective cation channel in M-1 mouse cortical collecting duct cells. J Membr Biol 146:29–45
29. Lefèvre CM, Diakov A, Haerteis S, Korbmacher C, Gründer S, Wiemuth D (2014) Pharmacological and electrophysiological characterization of the human bile acid-sensitive ion channel (hBASIC). Arch Eur J Physiol 466:253–263. https://doi.org/10.1007/s00424-013-1310-4
30. Lindorff-Larsen K, Piana S, Palmo K, Maragakis P, Klepeis JL, Dror RO, Shaw DE (2010) Improved side-chain torsion potentials for the Amber ff99SB protein force field. Proteins 78:1950–1958. https://doi.org/10.1002/prot.22711
31. Madej BD, Gould IR, Walker RC (2015) A parameterization of cholesterol for mixed lipid bilayer simulation within the Amber Lipid14 force field. J Phys Chem B 119:12424–12435. https://doi.org/10.1021/acs.jpcb.5b04924
32. Morris GM, Huey R, Lindstrom W, Sanner MF, Belew RK, Goodsell DS, Olson AJ (2009) AutoDock4 and AutoDockTools4: automated docking with selective receptor flexibility. J Comput Chem 30:2785–2791. https://doi.org/10.1002/jcc.21256
33. Páll S, Hess B (2013) A flexible algorithm for calculating pair interactions on SIMD architectures. Comput Phys Commun 184: 2641–2650. https://doi.org/10.1016/j.cpc.2013.06.003
34. Páll S, Abraham MJ, Kutzner C, Hess B, Lindahl E (2014) Tackling exascale software challenges in molecular dynamics simulations with GROMACS. In: Markidis S., Laure E. (eds) Solving Software Challenges for Exascale. EASC 2014. Lecture Notes in Computer Science, V. 8759. Springer, Cham
35. Paukert M, Babini E, Pusch M, Gründer S (2004) Identification of the Ca^{2+} blocking site of acid-sensing ion channel (ASIC) 1: implications for channel gating. J Gen Physiol 124:383–394. https://doi.org/10.1085/jgp.200308973
36. Pluhackova K, Kirsch SA, Han J, Sun L, Jiang Z, Unruh T, Böckmann RA (2016) A critical comparison of biomembrane force fields: structure and dynamics of model DMPC, POPC, and POPE bilayers. J Phys Chem B 120:3888–3903. https://doi.org/10.1021/acs.jpcb.6b01870

37. Rauh R, Diakov A, Tzschoppe A, Korbmacher J, Azad AK, Cuppens H, Cassiman JJ, Dotsch J, Sticht H, Korbmacher C (2010) A mutation of the epithelial sodium channel associated with atypical cystic fibrosis increases channel open probability and reduces Na^+ self inhibition. J Physiol 588:1211–1225. https://doi.org/10.1113/jphysiol.2009.180224
38. Sakai H, Lingueglia E, Champigny G, Mattei MG, Lazdunski M (1999) Cloning and functional expression of a novel degenerin-like Na^+ channel gene in mammals. J Physiol 519(Pt 2):323–333
39. Sanner MF (1999) Python: a programming language for software integration and development. J Mol Graph Model 17:57–61
40. Schaefer L, Sakai H, Mattei M, Lazdunski M, Lingueglia E (2000) Molecular cloning, functional expression and chromosomal localization of an amiloride-sensitive Na^+ channel from human small intestine. FEBS Lett 471:205–210
41. Schmidt A, Lenzig P, Oslender-Bujotzek A, Kusch J, Lucas SD, Gründer S, Wiemuth D (2014) The bile acid-sensitive ion channel (BASIC) is activated by alterations of its membrane environment. PLoS One 9:e111549. https://doi.org/10.1371/journal.pone.0111549
42. Schmidt A, Lohrer D, Alsop RJ, Lenzig P, Oslender-Bujotzek A, Wirtz M, Rheinstadter MC, Gründer S, Wiemuth D (2016) A cytosolic amphiphilic α-helix controls the activity of the bile acid-sensitive ion channel (BASIC). J Biol Chem 291:24551–24565. https://doi.org/10.1074/jbc.M116.756437
43. Siu SW, Pluhackova K, Böckmann RA (2012) Optimization of the OPLS-AA force field for long hydrocarbons. J Chem Theory Comput 8:1459–1470. https://doi.org/10.1021/ct200908r
44. Sun Y, Kollman PA (1995) Hydrophobic solvation of methane and nonbond parameters of the TIP3P water model. J Comput Chem 16:1164–1169. https://doi.org/10.1002/jcc.540160910
45. Trott O, Olson AJ (2010) AutoDock Vina: improving the speed and accuracy of docking with a new scoring function, efficient optimization, and multithreading. J Comput Chem 31:455–461. https://doi.org/10.1002/jcc.21334
46. Wassenaar TA, Pluhackova K, Böckmann RA, Marrink SJ, Tieleman DP (2014) Going backward: a flexible geometric approach to reverse transformation from coarse grained to atomistic models. J Chem Theory Comput 10:676–690. https://doi.org/10.1021/ct400617g
47. Wassenaar TA, Ingólfsson HI, Böckmann RA, Tieleman DP, Marrink SJ (2015) Computational lipidomics with insane: a versatile tool for generating custom membranes for molecular simulations. J Chem Theory Comput 11:2144–2155. https://doi.org/10.1021/acs.jctc.5b00209
48. Wiemuth D, Gründer S (2011) The pharmacological profile of brain liver intestine Na^+ channel: inhibition by diarylamidines and activation by fenamates. Mol Pharmacol 80:911–919. https://doi.org/10.1124/mol.111.073726
49. Wiemuth D, Sahin H, Falkenburger BH, Lefèvre CM, Wasmuth HE, Gründer S (2012) BASIC-a bile acid-sensitive ion channel highly expressed in bile ducts. FASEB J 26:4122–4130. https://doi.org/10.1096/fj.12-207043
50. Wiemuth D, Sahin H, Lefèvre CM, Wasmuth HE, Gründer S (2013) Strong activation of bile acid-sensitive ion channel (BASIC) by ursodeoxycholic acid. Channels (Austin) 7:38–42. https://doi.org/10.4161/chan.22406
51. Wiemuth D, Lefèvre CM, Heidtmann H, Gründer S (2014) Bile acids increase the activity of the epithelial Na^+ channel. Arch Eur J Physiol 466:1725–1733. https://doi.org/10.1007/s00424-013-1403-0
52. Yesylevskyy SO, Schäfer LV, Sengupta D, Marrink SJ (2010) Polarizable water model for the coarse-grained MARTINI force field. PLoS Comput Biol 6:e1000810. https://doi.org/10.1371/journal.pcbi.1000810